The DBCF-EM Gripper: Using Dual-Belt Curved-Flexure Eversion Mechanism Fingers for Confined-Space Robotic Grasping

A. E. Huisjes, J. H. B. Friederich, and J. L. Herder

***Abstract*—Conventional fingered grippers often struggle in confined spaces because limited lateral access prevents finger insertion and inward closing. This letter presents the DBCF-EM gripper, whose fingers combine a base-driven curved flexure, prescribing a tangential object-following trajectory, with a dual-belt eversion system that creates near-stationary contact surfaces and reduces sliding at the contact interfaces. This enables a low-disturbance caging grasp strategy in which the fingers propagate along the object surface rather than closing perpendicularly toward it. A prototype gripper was built for robotic tomato-removal experiments from a crate. Experiments showed contour following with a maximum deviation of 3 mm, negligible normal disturbance of at most 0.1 N, and a 91–97% reduction in tangential disturbance forces. In robotic trials, the gripper achieved 100% pick-up success and a 91% damage-free success rate, demonstrating its effectiveness for confined-space grasping.**

***Index Terms*—Grippers and other end-effectors, mechanism design, grasping, multifingered hands, robotics and automation in agriculture and forestry.**

I. Introduction

THE automation of agri-food product manipulation remains challenging because these products vary in shape, stiffness, and fragility [1]. Numerous robotic gripper concepts have therefore been developed for secure yet gentle handling while limiting excessive contact forces and contamination risk, including suction-based, puncturing, freezing, adhesive, universal/adaptive, parallel-jaw, and fingered approaches [1], [2]. Among these, fingered grippers are particularly attractive for delicate items with diverse properties, because they can realize robust grasps through form-closure while distributing contact and limiting local pressure peaks [3], [4], [5], or even avoid squeezing when caging strategies are used [6]. To further improve robustness, many fingered designs incorporate shape-adaptive principles [7], [8], [9], [10] and/or variable-stiffness mechanisms such as jamming and tensioned tendons [11], [12]. These grippers typically perform best when objects are laterally accessible, i.e., when sufficient free space surrounds the object to allow the fingers to approach from the sides.

However, conventional fingered grippers often fail in practical settings such as densely packed crates, hanging clusters, or narrow conveyor lanes [13], [14], because lateral space is limited or absent. Finger insertion and closing in confined spaces can excessively disturb neighboring items, causing grasp failure or damage. Existing solutions therefore often rely on advanced planning and obstacle interaction/avoidance strategies [15], [16], since these challenges typically arise during real-world deployment rather than during gripper design.

In this letter, we introduce and experimentally validate the Dual-Belt Curved-Flexure Eversion Mechanism (DBCF-EM) gripper for confined-space robotic grasping. The proposed gripper was designed and validated for a representative use case: automated one-by-one tomato removal from a densely packed crate. Rather than addressing this problem primarily through control, we propose a mechanical solution that limits environmental disturbance through the finger design itself. The finger design combines a curved, base-driven advancing flexure with a dual-belt eversion system.

Eversion-based robots are often soft, internally pressure-driven "length-growing" tubes or sleeves governed by membrane mechanics [17], [18]. Tendon- or belt-driven mechanisms, by contrast, transmit actuation through tensioned elements routed along the structure, enabling forward motion or steering without pneumatic pressurization [12]. Our approach differs from both: a curved, base-driven flexure prescribes a circular, tangential object-following trajectory while simultaneously driving dual-belt eversion motion, thereby creating near-stationary contact surfaces along the inner and outer contours and reducing friction at the contact interfaces. Together, these features enable a low-disturbance caging grasp strategy in which the fingers extend longitudinally from the gripper and propagate along the object surface rather than closing perpendicularly

Received 12 November 2025; accepted 21 March 2026. Date of publication 20 April 2026; date of current version 4 May 2026. This article was recommended for publication by Associate Editor M. Russo and Editor C. Gosselin upon evaluation of the reviewers' comments. This work was supported by Dutch Research Council under Grant P80401 Flexcraft. *(Corresponding author: A. E. Huisjes.)*

The authors are with the Faculty of Mechanical Engineering, Delft University of Technology, 2628, CD Delft, The Netherlands (e-mail: a.e.huisjes@tudelft.nl).

This article has supplementary downloadable material available at https://doi.org/10.1109/LRA.2026.3685468, provided by the authors.

Digital Object Identifier 10.1109/LRA.2026.3685468

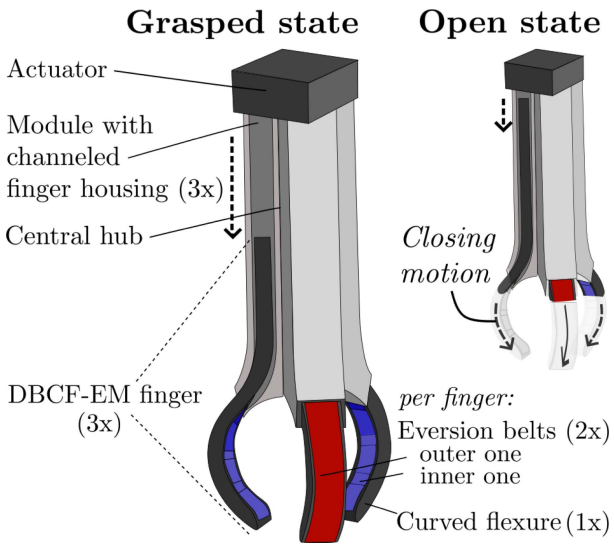

Fig. 1. Three-fingered DBCF-EM gripper in the open and grasped states. Unlike conventional grippers, its fingers follow a circular path defined by the curved flexures (black), enabling tangential object-following motion for confined-space grasping. Two everting belts (red, blue) maintain near-zero relative motion at the contact interface and reduce shear during motion.

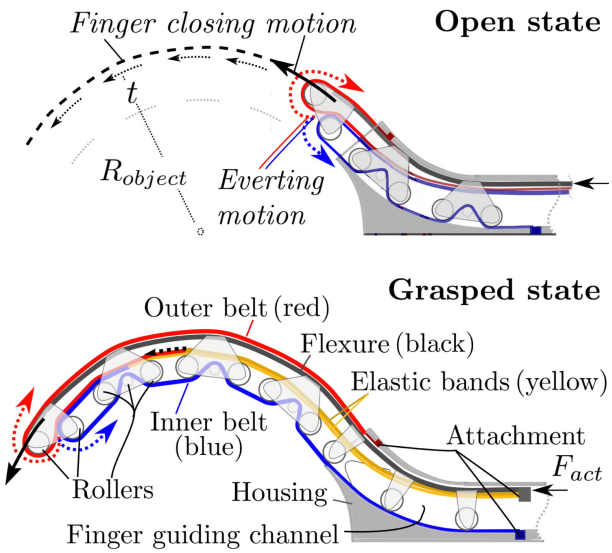

Fig. 2. Cross-sectional view of a DBCF-EM finger in the open and grasped states. Two everting belts (red, blue), guided by rollers, follow the curved flexure (black) and are fixed to the housing and flexure base via an elastic band (yellow). During grasp setting, the flexure is pushed outward the housing channel, restoring its curvature and following a circular path while driving the belts eversion motion from the tip along its outer sides to reduce shear with the environment.

toward it, requiring only minimal lateral clearance on the order of the finger thickness.

The paper is structured as follows. Section II describes the DBCF-EM concept, prototype fabrication, and pull-out force estimation. Section II-E details the experimental methods. Section III presents the experimental results. Sections IV and V discuss the findings and conclude the paper.

II. Method

A. Conceptual Gripper Design

Fig. 1 shows the three-fingered DBCF-EM gripper, and Fig. 2 shows a 2D cross-sectional sketch of a DBCF-EM finger, both in their **open** and **grasped** states, with the main components labeled. The gripper comprises three finger modules arranged around a central hub, each storing a DBCF-EM finger in a channeled housing. Each finger combines a pre-curved flexure (black) with a dual-belt eversion system consisting of an inner belt (blue) and an outer belt (red). The belts extend from the finger interior, pass over the fingertip in opposite directions, and cover the inner and outer curved finger surfaces, guided by rollers along the flexure contour. Each belt is fixed at the housing, while its free end is connected by a preloaded elastic band to the actuated end of the flexure.

The DBCF-EM fingers enable confined-space grasping through two disturbance-reducing principles: tangential object-following motion realized by the flexure design, and reduced tangential disturbance at the contact interfaces through the dual-belt eversion system. Their operation is described below.

1) Tangential Object-Following Finger Motion: A single actuator mounted on top of the hub drives all fingers synchronously by pushing the flexures outward from their base through the housings under the actuation force F_{act}. The flexures are pre-curved with a radius chosen to match the target object radius plus the finger thickness t. In the open state, they are retracted and straightened within the housings, with the flexures elastically deformed to conform to the internal channels. During grasp closing, each flexure advances through the channel, emerges from the housing, progressively recovers its original curvature, and follows a circular trajectory, allowing the finger to advance tangentially along the surface of the target spherical object during grasp acquisition.

The outward-curved housing outlets guide the fingers tangentially onto the object surface when the gripper is positioned with its longitudinal axis normal to that surface, while also allowing the finger modules to be placed closer together for a compact layout. As a result, the required object–environment clearance during grasp acquisition is limited mainly to the finger thickness, which is often available or can be created by gently displacing neighboring obstacles during finger passage.

More generally, the flexure forms the structural core of each finger, providing longitudinal stiffness for propagation through clutter, while its lateral bending compliance allows controlled deviation from the nominal path under gripper–object misalignment, obstruction by neighboring items, or slight object oversizing. This enables limited shape adaptivity within the elastic range without damaging the object.

2) Reduction of Tangential Disturbances: A flexure advancing along a surface would normally generate shear forces at the contact interface. In the proposed design, these are mitigated by combining the flexure with a dual-belt eversion system, as illustrated in Fig. 2. During grasp acquisition, rollers at the tip of the advancing flexure push against the inner wall of the wrapped belts. The belt portions within the center of the finger are thereby pulled forward at twice the flexure speed, elongating the attached elastic bands. Upon reaching the tip, they undergo eversion

motion and unwrap onto the curved flexure surfaces, covering them while becoming nearly stationary relative to the environment and thereby strongly reducing tangential disturbance. During object release, the process reverses: as the flexure retracts, the elastic bands pull the belts back from the exterior to the interior, thereby realizing inward eversion. Without these belts, the advancing finger would slide against the object and surrounding clutter, generating friction that could cause damage or misgrasps.

This principle is inspired by eversion mechanisms (EMs), which conventionally consist of a flexible inward-folded tube or membrane. Under internal overpressure, material is transported forward internally and redirected outward at the tip, such that the outer surface remains stationary relative to the environment while the mechanism extends longitudinally through eversion motion [17], [18]. The DBCF-EM realizes this principle in a mechanically driven planar form. Instead of internal pressure, the belts are driven by the advancing flexure. Unlike the typically straight propagation path of conventional EMs, the propagation path here is circular and prescribed by the flexure geometry. Additional rollers are therefore required to guide the belts along this contour and prevent shortcutting along the inner side between the fingertip and gripper wrist.

Beyond these two key grasp-acquisition features, the gripper must also retain the object once grasped, lifted, or manipulated by the robot. In the present multifunctional design, both the flexure and the belts contribute to this holding capability. The flexure forms the structural caging frame around the object, from which the holding force partly arises through its bending stiffness. The belts further enhance retention: the tensile stiffness of the inboard belt segments resists finger opening during pull-out, analogous to tendons in the human hand. The resulting caging strategy offers two advantages: no continuous actuation is required to maintain retention, and the object can be held with little squeezing because it is retained primarily through passive enclosure around its contour.

B. Analytical Models for Holding Force Prediction

To guide design, two first-order analytical models are presented for the per-finger holding force contributions of the form-closed caging grasp: one due to flexure bending stiffness and one due to eversion-belt tension. Both are expressed as functions of the enclosing angle ψ, which increases as the finger extends from the housing. The per-finger holding force is approximated as their sum, and the total gripper holding force as three times this value. As a first-order approximation, a rigid 2-D circular object of radius R is assumed, with longitudinal pull-out taken as the easiest escape direction and internal finger losses and object–finger friction neglected.

1) Holding Force of the Pre-Curved Flexure: The flexure contribution of one finger is estimated by solving the pull-out problem in Fig. 3 using a pseudo-rigid-body model (PRBM). Starting from the grasped state, in which a pre-curved flexure encloses a circular object, the object is pulled downward in small steps, causing the flexure to open and generate a tip contact force $\mathbf{F}_c$ acting normal to the object under the frictionless-contact

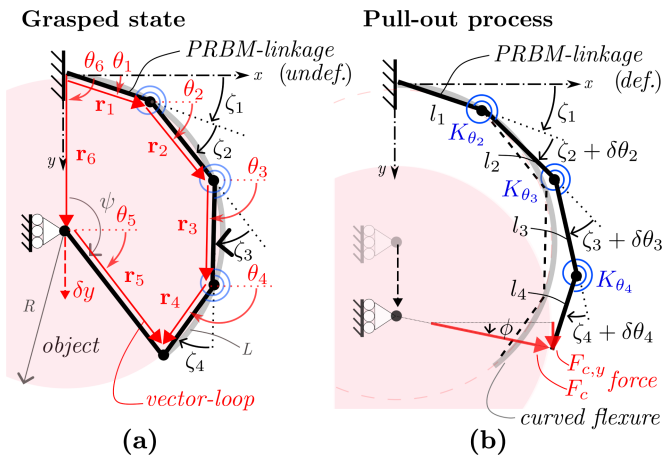

Fig. 3. Holding-force model for a single flexure. (a) Grasped state, with the pre-curved flexure enclosing the object. (b) During pull-out, the object moves downward in steps of δy, deflecting the flexure, modeled by a PRBM. For each step, the configuration follows from the vector loop $\mathbf{r}_1$–$\mathbf{r}_6$, and the retention force on the object is given by $-F_{c,y}$.

assumption. Its upward reaction component opposes pull-out and is taken as the retention force. The process ends when form closure is lost, and the maximum of $-F_{c,y}$ during pull-out is taken as the flexure holding-force contribution.

The flexure is modeled using the PRBM for initially curved beams in [19], which provides an analytical force–deflection approximation. It is represented as a 3R linkage with four serial links of lengths l_1–l_4, initial joint angles ζ_1–ζ_4, torsional springs at joints 2–4 ($K_{\theta 2}$–$K_{\theta 4}$), and a tip contact force $\mathbf{F}_c$ acting at angle ϕ, as shown in Fig. 3(b). Model parameters follow from the flexure geometry and material properties using the formulations in [19], with $L = \psi R$, and joint-angle deviations during object displacement denoted by $\delta\theta_1$–$\delta\theta_4$.

For each imposed pull-out step, the mechanism configuration is obtained from the closed vector loop

$$\mathbf{r}_1 + \mathbf{r}_2 + \mathbf{r}_3 + \mathbf{r}_4 = \mathbf{r}_5 + \mathbf{r}_6, \tag{1}$$

where $\mathbf{r}_1$–$\mathbf{r}_4$ denote the pseudo-links, $\mathbf{r}_5$ connects the object center to the flexure tip, and $\mathbf{r}_6$ describes the imposed object position. Among the kinematically admissible configurations, the physically realized one is taken as the minimum-energy state by minimizing the elastic potential energy stored in the torsional springs,

$$V = \frac{1}{2}K_{\theta 2}\,\delta\theta_2^2 + \frac{1}{2}K_{\theta 3}\,\delta\theta_3^2 + \frac{1}{2}K_{\theta 4}\,\delta\theta_4^2, \tag{2}$$

subject to the loop-closure constraint in (1). The constrained optimization is solved in MATLAB using `fmincon`.

For each pull-out step, the spring torque T_4 defines the contact force $\mathbf{F}_c$ through moment equilibrium of the fourth pseudo-link about its spring joint. Under the frictionless-contact assumption, $\mathbf{F}_c$ acts along θ_5, normal to the object surface. The flexure holding force is defined as the maximum value of $-F_{c,y}$ over the pull-out trajectory.

2) Holding Force of Belt Tension: The belt tension between the roller tabs, generated by the elongated elastic band, also

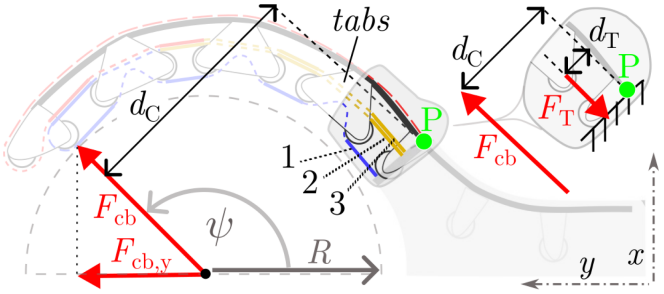

Fig. 4. Holding-force model for the belt-tension contribution. A moment balance about P relates F_{cb} at d_C to the tension $F_T = 3F_t$ in the three active belt segments between the wrist and first tab at d_T. The resulting retention force is $-F_{cb,y}$.

contributes to holding. Analogous to tendons in the human hand, this tension resists finger opening during object pull-out by opposing tab separation. In this first-order estimate, only the three dominant belt segments between wrist and first tab (1–3), shown in Fig. 4, are included, as they act closest to the wrist pivot and thus contribute most directly to the closing moment about P. Their contribution is estimated from a moment balance about P, with the segments modeled as pretensioned elements of equal tension F_t, giving a total tensile load $F_T = 3F_t$ at lever arm d_T, defined as the distance from the flexure to the roller axle minus one-third of the roller radius. This load opposes the fingertip contact force F_{cb}, yielding a retention force $-F_{cb,y}$. Frictional losses, tension redistribution, viscoelastic effects, and additional elastic-band extension during finger opening are neglected.

C. Use Case: Task and Design Requirements

To validate the DBCF-EM concept, a prototype gripper was designed to remove 33 piled tomatoes from a crate, one by one. The tomatoes had an average mass of 131 g (87–192 g), height of 62 mm (48–71 mm), and diameter of 60 mm (47–71 mm). The gripper was therefore tailored to average spherical tomatoes of 60 mm and 130 g, while remaining adaptable enough to handle the observed size range.

Tomatoes were chosen because they are representative of many spherical fruits in agri-food logistics, while also providing a demanding benchmark due to their fragility and dense packing. This makes the case well suited to derive and evaluate the functional requirements for confined-space grasping, where low-disturbance finger motion is essential. Although other products may require different dimensions or greater shape adaptability, the tomato-crate case captures a practically relevant and challenging design scenario.

D. Mechanical Design and Manufacturing

This section presents the mechanical design and manufacturing of the prototype gripper through photos of different assembly stages. Fig. 5 shows it in disassembled and assembled configurations, together with key dimensions. From top to bottom, it shows the finger components (a,b), the finger module in the partially and fully grasped states (c), the central hub (d), and the assembled gripper in the grasped state (e).

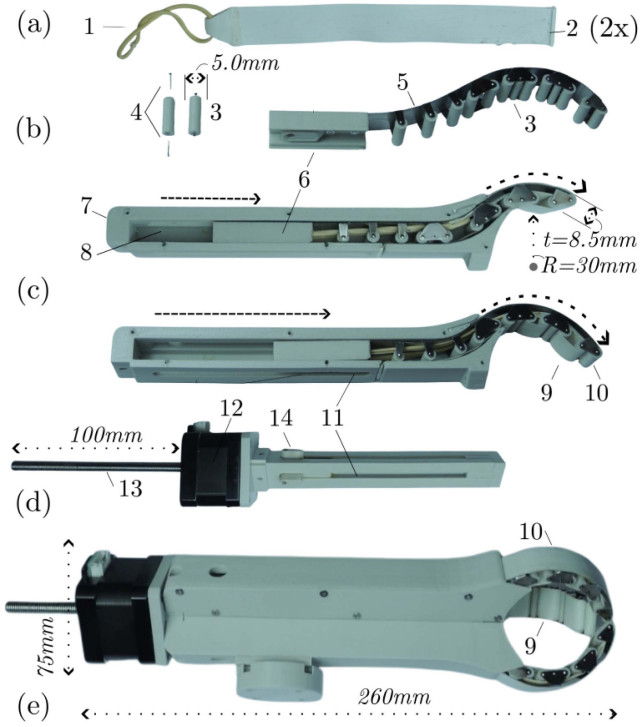

Fig. 5. Prototype of the DBCF-EM gripper during assembly. From top to bottom: (a,b) finger components, (c) the finger module in partially and fully grasped states, (d) the central hub, and (e) the assembled gripper.

The finger: As shown in (a) and (b), each finger comprises the belts (2) with elastic bands (1), the flexure (5) with rollers (3) and pins (4), and the actuation block (6). The flexure was CO_2-laser-cut from 0.2 mm hardened spring steel sheet (C100S, 1.1274, AISI 1095) and shaped into an S-configuration, with curvatures matching the channel (8) outlet contour and the object radius plus finger thickness. During passage through the channel exit, the flexure remains within its elastic range. The roller tabs were formed by locally softening the bending zones through torch heating followed by slow cooling, after which they were bent to 90°. These tabs hold the rollers, which are 3D-printed PLA cylinders mounted on 0.5 mm diameter, 8 mm long steel pins (4) that serve both as axles and as sliding interfaces within the housing channel.

The belts were 3D-printed from flexible TPU in three layers (0.2, 0.1, 0.1 mm) with alternating ±15° infill orientations, providing longitudinal stiffness and lateral flexibility. The elastic bands are rubber loops with an unstressed cross-section of 1.2×1.2 mm and total length of 56 mm, with tensile force increasing from 1.5 N at the 70 mm pre-tensioned length to 4.4 N at 150 mm in the fully grasped state. They are connected to the belts through a foldable printed tab welded back onto the belt to form a loop, as shown on the left. On the right; locally thickened tabs allow the belt to slide into and lock within slots inside the finger housing (7), as shown in (c). The actuation block (6) connects the elastic bands, secures the flexure base to the actuator, and guides the finger through the channel.

The finger module, central hub, & gripper: The finger module (c) contains a housing (7) with a channel (8) for the finger

and slots for belt attachment, enclosed by a lid (see (e)). A longitudinal slot (11) in each housing aligns with one face of the central hub during assembly. In (c), the lid is omitted to reveal the stored finger, with the belts covering its inner (9) and outer (10) contours and routed over the rollers. As the flexure advances, the finger extends from the housing while the belts evert at the tip, transitioning from the partially grasped state (top (c)) to the fully grasped state (bottom (c)).

The central hub (d) consists of a hollow triangular bar with side slots (11). Inside, a slider (14) moves axially, driven by a T6× 2 spindle (13) rotated by the actuator (12). The slider has three protrusions passing through the slots and connecting to the finger actuation blocks (6), thereby driving all fingers synchronously. The actuator is a NEMA 17 motor with a holding torque of 0.26 Nm, powered by an A4988 stepper driver connected to an Arduino. Under the selected settings, the gripper opened and closed in approximately 8 s (1 cm/s finger extrusion), chosen for quasi-static validation but reducible by a factor of three in practical use.

The fully assembled gripper in the grasped state (e), measures 260 mm in length and 75 mm in width, with a total mass of 431 g, of which 269 g is due to the actuator and spindle. Each finger measures 8.5 mm in thickness and 15 mm in width.

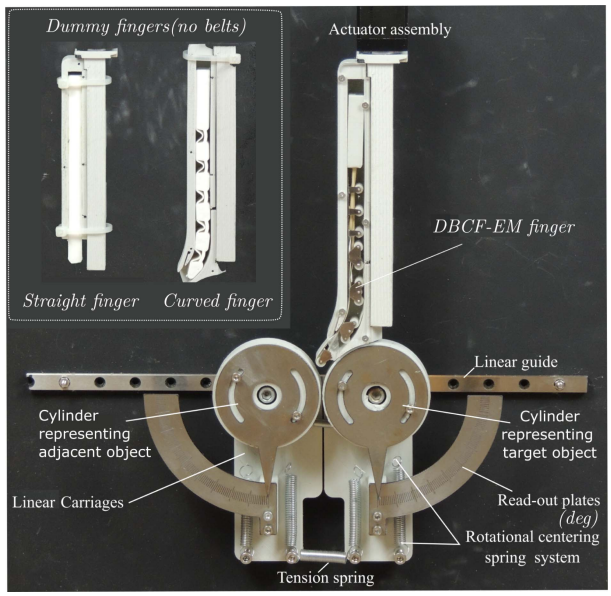

Fig. 6. Setup for measuring tangential disturbance during finger insertion. Two cylinders on spring-coupled carriages rotate and translate as the finger passes between them. Force is obtained from angular disk rotation (°) using the cylinders' rotational spring stiffness. A straight and a curved dummy finger without everting belts are included for comparison.

E. Experimental Performance Validation

To evaluate the gripper's effectiveness for confined-space grasping, six performance metrics were assessed using dedicated experiments. All experiments were performed at low actuation speed to ensure quasi-static behavior.

1) Tangential Object-Following Finger Motion: The finger should follow the object tangentially, without measurable deviation (mm), such that environmental perturbation is limited to the finger thickness. This was evaluated using side-view video recordings of a single finger grasping an object of mean diameter $D = 60$ mm. Stills at successive time points were overlaid to visualize deviations from the object surface and the final finger state.

2) Tangential Disturbances At Contact Interfaces: To assess the effectiveness of the dual eversion belts system, tangential disturbances during finger insertion were measured using the setup in Fig. 6. An advancing finger passes between two cylinders representing a target and adjacent object. In a real pile, finger insertion causes coupled normal and tangential interactions, resulting in translation, rotation, or load redistribution depending on local constraints. The present setup is intentionally simplified to isolate the tangential shear component specifically targeted by the belts. Object rotation serves as a direct readout, since tangential shear generates a moment at the contact interface. Longitudinal translation is constrained and evaluated separately, as it arises from coupled normal and tangential interactions rather than belt-induced shear alone.

The setup comprises two cylinders ($R = 30$ mm) mounted on ball-bearing axles and free-running carriages along a linear guide. The carriages are coupled by an extension spring providing an effective force of 7 N at the nominal finger thickness of 11 mm. Each cylinder is centered by opposing springs ($\kappa_{\text{obj}} = 0.66$ mNm/deg, $\kappa_{\text{obst}} = 0.64$ mNm/deg), and the maximum angular perturbation $\Delta\theta_{\max}$ is converted to peak tangential force using the calibrated rotational spring stiffness.

Ten DBCF-EM trials were averaged and compared with two beltless dummy fingers (shown in Fig. 6), one straight and one curved. Both matched the DBCF-EM in thickness and contact material to ensure comparable friction. Peak-force reduction was evaluated separately for the target and adjacent object.

3) Holding Force: Holding force, relevant for vertical object removal from the pile, was measured in by mounting the gripper vertically upward and closed around a spherical object ($D = 60$ mm, $m_{\text{obj}} = 50$ g), which was pulled upward with a spring scale until release. The maximum measured force, read with a precision of ± 25 g ($\approx \pm 0.25$ N), was corrected for the object weight (≈ 0.5 N) to obtain the net holding force.

4) Net Disturbance Force on the Object During Grasping: Excessive longitudinal interaction forces between the advancing fingers and the object during grasp acquisition can push the object away and cause misgrasps. To quantify this net disturbance force, a spherical object ($D = 60$ mm) was mounted on a linear slider and centered by two opposing springs with an effective stiffness of $k_{\text{eff}} = 0.19$ N/mm. The gripper was aligned with the slider at a 2 mm wrist-to-object clearance. During repeated grasping cycles, the maximum object displacement Δu was recorded with a precision of ± 0.25 mm, and the corresponding net disturbance force was calculated as $|F_{\text{net}}| = k_{\text{eff}}\Delta u$.

5) Grasp Success Rate in a Practical Robotic Set-Up: Grasp success rate was evaluated in a practical robotic setting by integrating the gripper into the system shown in Fig. 7 and removing 33 piled tomatoes one by one. A successful grasp required both removal from the pile and damage-free handling.

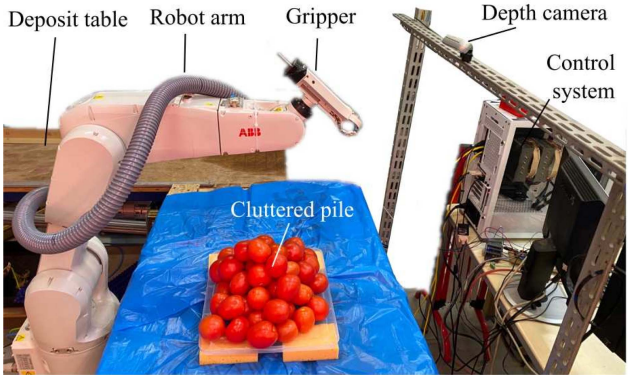

Fig. 7. Robotic setup for grasp-success-rate evaluation, showing automated tomato removal from a crate by a robotic arm positioning the gripper above each target.

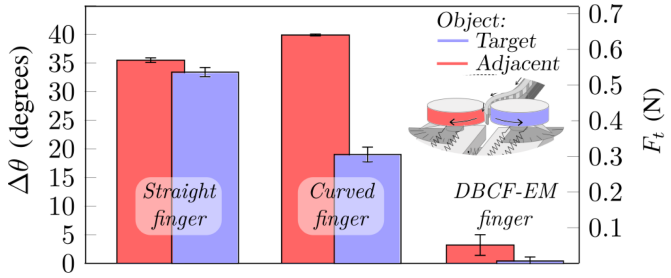

Fig. 8. Tangential disturbance results at the target (blue) and adjacent (red) object interfaces, shown as rotation (left axis) and corresponding force (right axis). The DBCF-EM finger causes lower disturbances than the two dummy fingers.

For each attempt, a tomato at the pile surface was selected by visual detection, and the robot positioned the gripper vertically above the estimated object center with an accuracy of ± 5 mm in both horizontal and vertical directions. The gripper was then actuated to enclose the object, after which the robot lifted it from the pile and placed it on a deposit table for release. Grasp success and damage rates were determined from video recordings and visual inspection.

The setup used an ABB IRB 1200 robotic arm controlled via ROS and stereo vision for tomato detection and position estimation, as developed in [20], but here used without the advanced software implementations presented there. Apart from target position estimation, no higher-level obstacle recognition or grasp-pose planning was used; the gripper approached each target top-down, without planned reorientation toward local voids to reduce finger–object contact.

6) Grasping a Variety of Object Types: We performed an exploratory grasping experiment in which the gripper picked up various test objects from a table. As shown in Fig. 9, the set included rigid 3D-printed objects with round and square geometries in different sizes, as well as a pawn-shaped variant. To assess performance on deformable items, a massage ball and two highly pliable toy objects were also included.

III. Results and Implications

This section presents the experimental outcomes for the six defined performance metrics and their implications.

1) Tangential Object-Following Finger Motion: Overlaid side-view stills showed that the finger advanced tangentially along a spherical object with less than 3 mm deviation during the first 10 mm after exiting the wrist, then closely followed the contour until full enclosure. No significant outward bending was observed on contact. This confirms tangential, object-following grasp formation with clearance near the finger thickness, and shows that curved, base-driven flexures can realize such circular trajectories.

2) Tangential Disturbances At Contact Interfaces: Fig. 8 shows the tangential disturbances at the target (blue) and adjacent (red) object interfaces for the straight dummy, curved dummby, and DBCF-EM fingers. The left axis gives the maximum angular perturbation $\Delta\theta$ during insertion, and the right axis the corresponding tangential force F_t from the stiffness relation in Section II-E. Over $n = 10$ trials, the mean target/adjacent rotations were $35.5^\circ/33.5^\circ$ for the straight finger, $39.9^\circ/19.1^\circ$ for the curved finger, and only $3.2^\circ/0.5^\circ$ for the DBCF-EM finger. This corresponds to disturbance reductions of at least 91% and 97% relative to the dummy fingers, confirming that the dual eversion belts strongly suppress tangential shear while advancing between two obstacles.

3) Holding Force: The pull-out tests yielded a holding force of $F_h = 3.7 \pm 0.4$ N (95% CI, $n = 7$). The analytical models predict 0.072 N per finger for the flexure contribution (0.22 N for three fingers). For a measured pretension of $F_t = 3$ N ($F_T = 9$ N), lever arms $d_C = 42$ mm and $d_T = 4.33$ mm, and $\psi = 135^\circ$, the belt model predicts 0.66 N per finger (1.98 N for three fingers). Together, both models explain 2.20 N, or $\approx 59\%$, of the measured value. The difference is likely due in part to the simplifying assumptions, including neglecting internal mechanism friction and object–finger friction.

4) Net Disturbance Force on the Object During Grasping: The net disturbance force during grasping was measured as $F_{\text{net}} = 0.1 \pm 0.04$ N (95% CI, $n = 10$). This is negligible compared to both the holding force and the object weight, indicating it is unlikely to damage or displace the object outward during grasping. The low value is consistent with the observed tangential finger motion and absence of notable flexure bending in the first experiment.

5) Grasp Success Rate in a Practical Robotic Set-Up: The gripper successfully removed all 33 tomatoes, yielding a raw grasp success rate of 100% (33/33). Post-experiment inspection identified three damaged tomatoes, resulting in an effective grasp success rate of 90.9% (30/33). The supplementary video illustrates the robotic grasping process. Due to perishability and practical test constraints, only the first robotic run is reported, although additional runs showed similar trends.

The damage consisted of localized skin punctures rather than bruising or tearing, and is attributed to geometric details of the current prototype, such as uncovered flexure edges and the sharp-edged housing exit, rather than to failure of the caging-grasp principle, flexure propagation, or the eversion concept. This suggests that the grasping concept and the mechanism principles are effective, but that local edge rounding or coverage is needed to prevent damage during insertion.

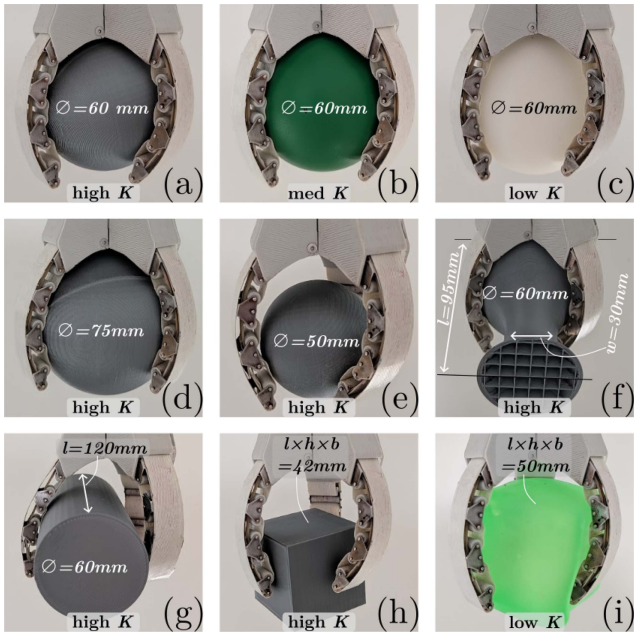

Fig. 9. Grasping of various test objects: spheres (a–e), a pawn-shaped object (f), a round rod (g), a square block (h), and a soft square block (i). Dimensions are indicated in the figure. Grey objects are rigid 3D prints; (b) is a medium-stiff massage ball, and (c) and (i) are highly pliable toys.

6) Grasping a Variety of Object Types: As shown in Fig. 9, all test objects could be grasped and lifted, although grasp quality and stability varied with geometry and stiffness. Performance was best for the sphere-like objects, for which the curved fingers could follow the contour and form a well-enclosed cage. The larger sphere caused gradual outward finger deflection while the smaller object has mobility but remain within the case. The pawn-shaped object benefited from simple object-dependent placement that avoided routing around the elongated protrusion. The massage ball and pliable toy were also grasped with little visible compression, highlighting the low-squeezing nature of the caging principle.

The elongated round rod was liftable but often rested on the roller tabs, with only one finger conforming, resulting in lower stability. Such geometries may benefit from a different finger arrangement, e.g., a 1-opposed-to-2 configuration aligned with the object axis. The rigid square block was most challenging, as the fingers could not reliably tuck underneath to form a form-closed cage, making the grasp friction-dependent and disturbance-sensitive. In contrast, the soft square block was grasped more reliably, likely because the fingers could partially nest into it and friction increased.

IV. Discussion

This study introduced a gripper concept for confined-space grasping in which the fingers follow a tangential, object-following trajectory rather than approaching the object normal to its surface. The experiments showed that the DBCF-EM fingers can realize this motion with low disturbance: tangential shear at the contact interfaces was reduced by 91–97% relative to the dummy fingers, while net object disturbance during grasp formation remained low ($F_{net} = 0.1$ N). In robotic validation, this enabled successful removal of all 33 tomatoes, with an effective damage-free success rate of 90.9%.

These results position the DBCF-EM as a distinct hardware-oriented approach to confined-space grasping. The proposed gripper introduces capabilities not commonly offered by existing designs, most notably tangential object-following finger motion and low-disturbance grasp acquisition in access-constrained environments. Accordingly, the aim of this study was not a direct benchmark against conventional grippers on generic metrics alone, but the realization and validation of this new mechanical concept and its functional behavior. Broader positioning within the literature is therefore more appropriate than strict head-to-head comparison.

Rather than relying primarily on perception, planning, or precise control, part of the grasping complexity is embedded in the gripper mechanism itself: the fingers act as passive self-searching devices that maneuver around the object through interaction. Simple vertical positioning above a tomato was sufficient for the fingers to route through clutter, requiring top rather than lateral access. This is particularly relevant in dense piles, where collision-free trajectories are difficult to plan.

From a mechanical perspective, integrating flexures provides shape adaptability, a defined trajectory, and greater load-bearing capability than many soft or pressure-driven systems. Moreover, unlike many non-caging grippers that rely on object resistance for finger conformation and on continuous actuation forces for retention, the DBCF-EM aims to retain the object primarily through passive geometric enclosure, with limited squeezing, so that retention is governed mainly by design rather than actuation force.

Holding force and design implications: The measured holding force was sufficient for the present use case under quasi-static conditions. In pull-out tests, the gripper generated 3.7 N, about twice the weight of the heaviest tomatoes. For our use case, this value is likely conservative, since real tomatoes resisted sliding more strongly than the dummy objects. However, it remains modest for faster industrial handling.

The analytical models help interpret this result and identify the most influential design parameters. For the present geometry, the modeled flexure contribution is small relative to the belt contribution, suggesting that belt pretension is the dominant modeled retention mechanism, although this may be somewhat overestimated because routing losses were neglected.

Belt pretension increases the modeled holding force linearly, but also raises actuation force and may cause inward finger pre-deflection. The flexure contribution is more sensitive to geometric changes: according to the model, it increases from about 0.22 N to ≈ 0.8 N for the three-finger gripper when the enclosing angle increases to $\psi = 180^\circ$ at the same thickness, and to ≈ 1.8 N when the flexure thickness is doubled from $t = 0.2$ mm to $t = 0.4$ mm at comparable $\psi = 135^\circ$. These trends show that a higher holding force is feasible, but introduces trade-offs with compliance, adaptability, and actuation force, motivating integrated optimization of flexure and belt parameters. More broadly, the same PRBM-based framework could be extended to estimate squeezing forces on oversized objects or to analyze the path and interaction forces of advancing fingers during confined-space navigation.

Remaining challenges and future work: The experimental validation was use-case specific and performed only on tomatoes under quasi-static conditions. Tomatoes were chosen because they are representative of many spherical fruits in agri-food logistics, while also providing a demanding benchmark due to their fragility and dense packing. However, exploratory tests with additional object shapes and stiffnesses suggest that the DBCF-EM concept can be extended beyond this use case, provided that the finger geometry and arrangement are tailored to the object class.

Despite the fragility of the tomatoes, the concept performed well. The remaining object damage is an important topic for future development, but the results suggest that it is mainly related to prototype embodiment rather than the underlying mechanism principles. Likely improvements include refined exit edge rounding and shielding the sharp flexure edges using protective covers or slightly wider belts. In addition, practical metrics such as cycle time, robustness, hygiene, and lifetime remain important for industrial adoption. Replacing the belts with a fully enclosing eversion sleeve around the flexure is a promising next step, as it could reduce damage risk and improve hygiene, robustness, and durability while preserving the same underlying mechanism principles.

More broadly, to the best of our knowledge, the DBCF-EM finger represents the first flexure-driven eversion mechanism, in contrast to conventional pressure-driven eversion designs. The results suggest wider potential for combining flexures with eversion principles to achieve predictable motion, load-carrying capability, and safe interaction in dense and delicate environments. Beyond food handling, such mechanisms may also be relevant for medical devices, inspection tools, and search-and-rescue robots.

V. Conclusion

This article introduced the Dual-Belt Curved-Flexure Eversion Mechanism (DBCF-EM), a novel flexure-driven eversion mechanism implemented as gripper fingers for confined-space grasping. The concept combines a base-driven curved flexure, which prescribes a tangential object-following trajectory, with a dual-belt eversion system that creates near-stationary contact surfaces and thereby reduces sliding at the contact interfaces. This enables a low-disturbance caging grasp strategy in which the fingers propagate along the object surface rather than closing perpendicularly toward it.

For validation, a prototype gripper was designed and built for automated one-by-one removal of piled tomatoes. Technical experiments, robotic validation, and two analytical holding-force models were used to evaluate its distinctive hardware capabilities. The results showed that the fingers followed the object contour with a maximum deviation of 3 mm and induced only a negligible net disturbance force of 0.1 N during grasp formation. The dual-belt eversion system reduced tangential disturbances by 91–97% compared with dummy fingers, confirming effective shear suppression while advancing between adjacent objects. The measured holding force of 3.7 N was sufficient for quasi-static removal in the intended use case, while the analytical models explained about 60% of this value. In robotic validation, the gripper removed all 33 tomatoes from a crate using simple vertical positioning above each target, with an effective damage-free success rate of 91%, with the remaining failures related to prototype embodiment rather than the underlying grasping principle.

Together, these results demonstrate that the proposed confined-space caging concept and its DBCF-EM embodiment offer a distinct hardware-oriented approach to confined-space grasping, shifting part of the grasping complexity from planning and control to the mechanism itself.

References

[1] B. Zhang, Y. Xie, J. Zhou, K. Wang, and Z. Zhang, "State-of-the-art robotic grippers, grasping and control strategies, as well as their applications in agricultural robots: A review," *Comput. Electron. Agriculture*, vol. 177, 2020, Art. no. 105694.

[2] Z. Samadikhoshkho, K. Zareinia, and F. Janabi-Sharifi, "A brief review on robotic grippers classifications," in *Proc. IEEE Can. Conf. Elect. Comput. Eng.*, 2019, pp. 1–4.

[3] J. Hernandez et al., "Current designs of robotic arm grippers: A comprehensive systematic review," *Robotics*, vol. 12, no. 1, 2023, Art. no. 5.

[4] L. Birglen, "Enhancing versatility and safety of industrial grippers with adaptive robotic fingers," in *Proc. IEEE/RSJ Int. Conf. Intell. Robots Syst.*, 2015, pp. 2911–2916.

[5] Y.-J. Kim, H. Song, and C.-Y. Maeng, "BLT gripper: An adaptive gripper with active transition capability between precise pinch and compliant grasp," *IEEE Robot. Automat. Lett.*, vol. 5, no. 4, pp. 5518–5525, Oct. 2020.

[6] D. Kim, Y. Maeda, and S. Komiyama, "Caging-based grasping of deformable objects for geometry-based robotic manipulation," *ROBOMECH J.*, vol. 6, pp. 1–13, 2019.

[7] C. Meijneke, G. Kragten, and M. Wisse, "Design and performance assessment of an underactuated hand for industrial applications," *Mech. Sci.*, vol. 2, no. 1, pp. 9–15, 2011.

[8] R. A. Stavenuiter, L. Birglen, and J. L. Herder, "A planar underactuated grasper with adjustable compliance," *Mechanism Mach. Theory*, vol. 112, pp. 295–306, 2017.

[9] J. Hughes, U. Culha, F. Giardina, F. Guenther, A. Rosendo, and F. Iida, "Soft manipulators and grippers: A review," *Front. Robot. AI*, vol. 3, 2016, Art. no. 69.

[10] Z. Wang and S. Hirai, "A soft gripper with adjustable stiffness and variable working length for handling food material," in *Proc. IEEE Int. Conf. Real-time Comput. Robot.*, 2018, pp. 25–29.

[11] B. Fang et al., "Multimode grasping soft gripper achieved by layer jamming structure and tendon-driven mechanism," *Soft Robot.*, vol. 9, no. 2, pp. 233–249, 2022.

[12] R. Ma and A. Dollar, "Yale OpenHand project: Optimizing open-source hand designs for ease of fabrication and adoption," *IEEE Robot. Automat. Mag.*, vol. 24, no. 1, pp. 32–40, Mar. 2017.

[13] C. W. Bac, J. Hemming, B. van Tuijl, R. Barth, E. Wais, and E. J. van Henten, "Performance evaluation of a harvesting robot for sweet pepper," *J. Field Robot.*, vol. 34, no. 6, pp. 1123–1139, 2017.

[14] J. R. Davidson, A. Silwal, C. J. Hohimer, M. Karkee, C. Mo, and Q. Zhang, "Proof-of-concept of a robotic apple harvester," in *Proc. IEEE/RSJ Int. Conf. Intell. Robots Syst.*, Oct. 2016, pp. 634–639.

[15] Y. Xiong, Y. Ge, and P. J. From, "Push and drag: An active obstacle separation method for fruit harvesting robots," in *Proc. IEEE Int. Conf. Robot. Automat.*, 2020, pp. 4957–4962.

[16] E. Páll and O. Brock, "Analysis of open-loop grasping from piles," in *Proc. Int. Conf. Robot. Automat.*, 2021, pp. 2591–2597.

[17] L. Blumenschein, M. Coad, D. Haggerty, A. Okamura, and E. Hawkes, "Design, modeling, control, and application of everting vine robots," *Front. Robot. AI*, vol. 7, 2020, Art. no. 548266.

[18] S. Al Harthy et al., "Tip-growing robots: Design, theory, application," *IEEE Trans. Robot.*, vol. 41, pp. 5511–5532, 2025.

[19] V. K. Venkiteswaran and H.-J. Su, "A versatile 3R pseudo-rigid-body model for initially curved and straight compliant beams of uniform cross section," *J. Mech. Des.*, vol. 140, no. 9, 2018, Art. no. 092305.

[20] R. Raja, A. K. Burusa, G. Kootstra, and E. J. Van Henten, "Advanced robotic system for efficient pick-and-place of deformable poultry in cluttered bin: A comprehensive evaluation approach," *IEEE Trans. AgriFood Electron.*, vol. 2, no. 2, pp. 355–371, Sep./Oct. 2024.